J Mol Model (2013) 19:4823–4836
DOI 10.1007/s00894-013-1952-3

ORIGINAL PAPER

DFT and docking studies of rhodostreptomycins A and B and their interactions with solvated/nonsolvated Mg^{2+} and Ca^{2+} ions

Christiaan Jardínez · Ines Nicolás-Vázquez · Julian Cruz-Borbolla · Cesar A. González-Ramírez · Miguel Cepeda · Jose Correa-Basurto · Thangarasu Pandiyan · Rene Miranda

Received: 3 January 2013 / Accepted: 17 July 2013 / Published online: 13 September 2013

Abstract The interactions of L-aminoglucosidic stereoisomers such as rhodostreptomycins A (Rho A) and B (Rho B) with cations (Mg^{2+}, Ca^{2+}, and H^{+}) were studied by a quantum mechanical method that utilized DFT with B3LYP/6-311G**. Docking studies were also carried out in order to explore the surface recognition properties of L-aminoglucoside with respect to Mg^{2+} and Ca^{2+} ions under solvated and nonsolvated conditions. Although both of the stereoisomers possess similar physicochemical/antibiotic properties against *Helicobacter pylori*, the thermochemical values for these complexes showed that its high affinity for Mg^{2+} cations caused the hydration of Rho B. According to the results of the calculations, for Rho A–$Ca^{2+}(H_2O)_6$, $\Delta H = -72.21$ kcalmol^{-1}; for Rho B–$Ca^{2+}(H_2O)_6$, $\Delta H = -72.53$ kcalmol^{-1}; for Rho A–$Mg^{2+}(H_2O)_6$, $\Delta H = -72.99$ kcalmol^{-1} and for Rho B–$Mg^{2+}(H_2O)_6$, $\Delta H = -95.00$ kcalmol^{-1}, confirming that Rho B binds most strongly with hydrated Mg^{2+}, considering the energy associated with this binding process. This result suggests that Rho B forms a more stable complex than its isomer does with magnesium ion. Docking results show that both of these rhodostreptomycin molecules bind to solvated Ca^{2+} or Mg^{2+} through hydrogen bonding. Finally, Rho B is more stable than Rho A when protonation occurs.

Keywords DFT study · Rhodostreptomycins A and B · Mg^{2+}, Ca^{2+} and H^{+} ions

C. Jardínez · J. Cruz-Borbolla (✉) · C. A. González-Ramírez
Área Académica de Química, Universidad Autónoma del Estado de Hidalgo, Unidad Universitaria, Km 4.5 Carretera Pachuca-Tulancingo, 42184 Pachuca, Hidalgo, Mexico
e-mail: jcruzborbolla@yahoo.com.mx

I. Nicolás-Vázquez · R. Miranda
Departamento de Ciencias Químicas de la Facultad de Estudios Superiores Cuautitlán Campo 1, Universidad Nacional Autónoma de México, Cuautitlán Izcalli, Estado de México 54740, Mexico

T. Pandiyan
Facultad de Química, Universidad Nacional Autónoma de México (UNAM), Ciudad Universitaria, Coyoacán 04510 México D.F., Mexico

M. Cepeda · J. Correa-Basurto
Laboratorio de Modelado Molecular y Bioinformática, Sección de Estudios de Posgrado e Investigación, Escuela Superior de Medicina, Instituto Politécnico Nacional, Plan de San Luis y Díaz Mirón, 11340 México City, Mexico

Introduction

Recently, the stereoisomeric L-aminoglucosides rhodostreptomycin A (with the *R* configuration; Rho A) and rhodostreptomycin B (with the *S* configuration; Rho B; see Scheme 1) were isolated from co-culture broths of *Rhodococcus* 307CO [1]. It is known that Rho A and Rho B exhibit considerable antibiotic activity against the cell growth of *Helicobacter pylori*, which is a known promoter of gastrointestinal cancer [1]. Importantly, the probability of developing stomach cancer increases in humans over the age of 50 years old [2].

One of the current challenges for the pharmaceutical industry is to biologically synthesize active compounds, through phytochemical processes or interactions of different microbial organisms [3–5], that can inhibit highly resistant microbial infections such as MRSA (methicillin-resistant *Staphylococcus aureus*) and VREF (vancomycin-resistant *Enterococcus faecium*) [6–10]. In particular, the use of different microorganisms is becoming a common strategy for preparing biologically active compounds [11–14]. On the other hand, in silico studies can be used [15–17] to analyze the experimental conditions under which it is possible to synthesize a particular

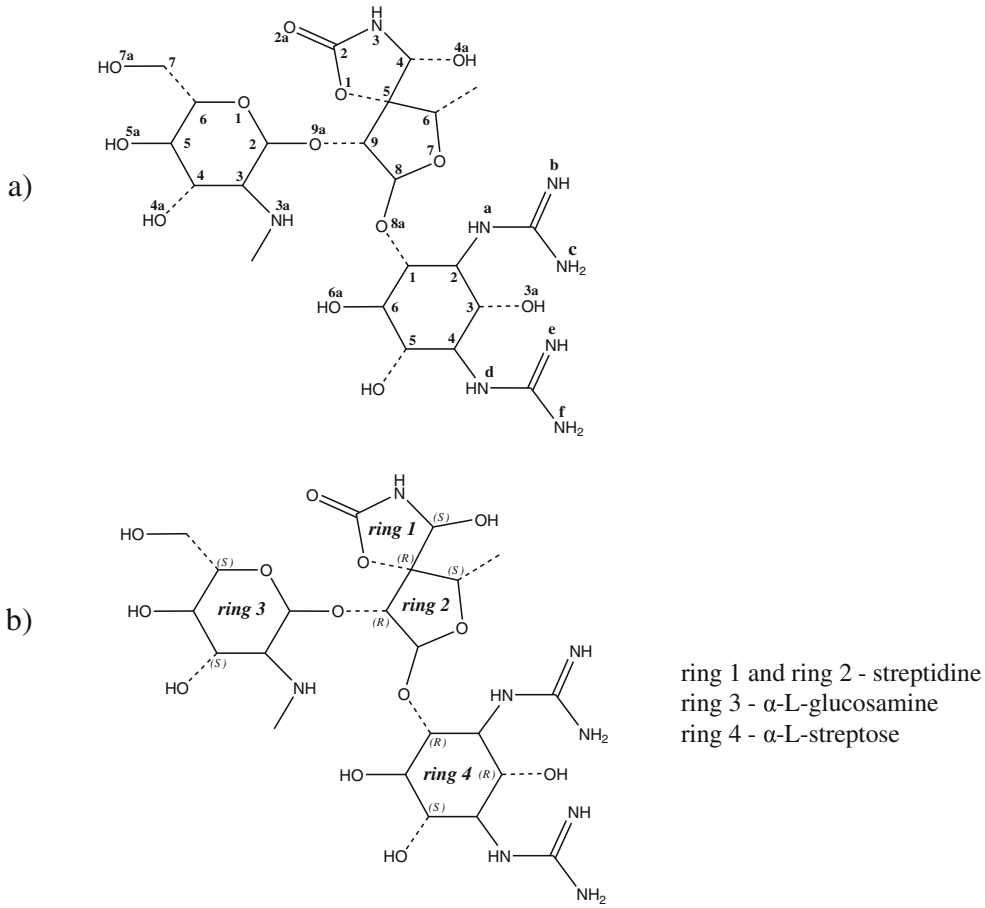

Scheme 1 Chemical structures of **a** rhodostreptomycin A and **b** rhodostreptomycin B, showing the atom and ring numbering schemes used and the stereogenic carbon centers

compound that is expected to have specific antimicrobial properties [18, 19]. Applying such an approach can circumvent the tedious process of experimentally deriving the appropriate antibiotic formulation [20–22]. Thus, computational chemistry is often employed to determine and analyze the structural stabilities and expected antimicrobial activities of target molecules [15, 23]. Furthermore, it is also important to mention that previous studies of antibiotics have suggested that their potency increases when they interact with Ca^{2+} or Mg^{2+} [16, 18]. Consequently, theoretical methods have been used to analyze several L-aminoglucoside antibiotics in the presence of Ca^{2+} and Mg^{2+} ions as a possible means to increase their stability [24, 25] through coordination with water molecules [26, 27]. Moreover, water molecules are involved with ligand recognition; this concept has been explored using docking procedures [28]. Thus, in the work described in the present paper, we theoretically examined the molecular interactions of the antibiotics Rho A and B with Ca^{2+} and Mg^{2+} ions in order to calculate their coordination properties and—using these theoretical data—infer their antibiotic efficiencies against *Helicobacter pylori*. Additionally, enthalpy calculations (utilizing quantum mechanics, QM) of Rho A and B with these solvated metals (Ca^{2+} and Mg^{2+}) were performed to determine the main surface contact zones of the molecules.

Methodology

Total optimization of the molecular models was performed for both the neutral and protonated forms of the rhodostreptomycins A and B using the Gaussian 09 program [29]. The interactions of these stereoisomers with Ca^{2+} and Mg^{2+} ions were analyzed by applying density functional theory (DFT) with the basis set 6-311G** for all atoms. The B3LYP exchange-correlation functional was employed [30–32]. This method provides suitable structural and electronic parameters for Ca(II)/Mg(II) compounds [33]. Total structure optimization along with vibrational analysis of the optimized structures was performed in order to determine

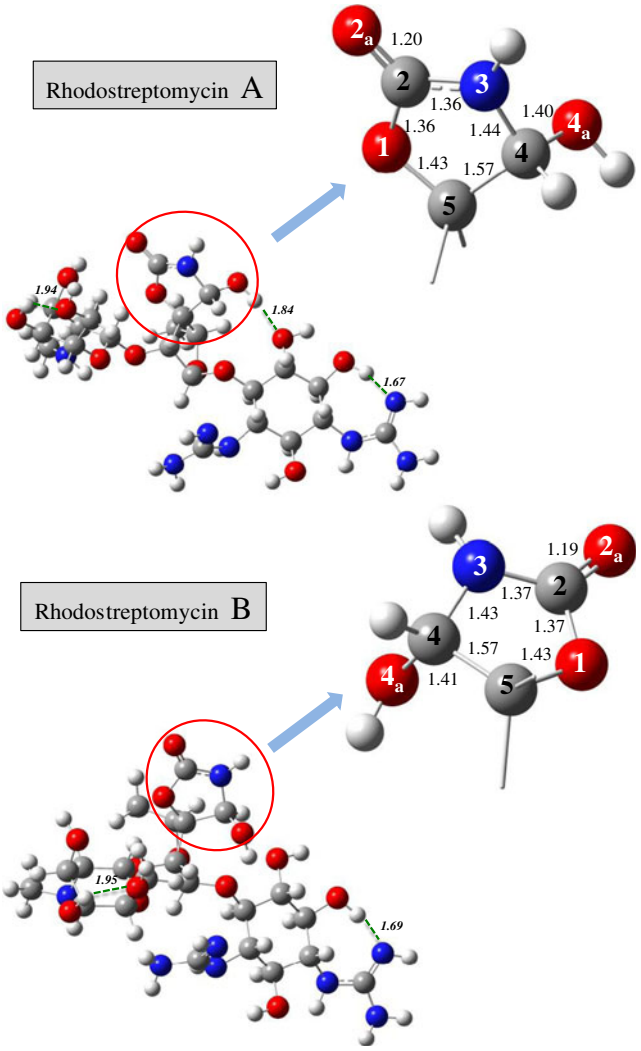

Fig. 1 Optimized geometries (shown in 3D) for Rho A and B. Some bond lengths (in Å) are shown for the oxazolidinone ring (ring 1) as well as some hydrogen bonds, all of which were calculated using B3LYP/6-311G **

whether each structure corresponded to a maximum or a minimum on the potential energy curve. Molecular geometries were optimized using B3LYP/6-311G** in an aqueous medium (dielectric constant ε = 78.39) by means of the PCM method [34]. The calculated binding energies (BE) between each rhodostreptomycin structure and Ca^{2+} or Mg^{2+} were corrected for the zero-point energy (ZPE).

The stereostructures of the rhodostreptomycins are shown in Scheme 1, which highlights the different Cahn–Ingold–Prelog [35] configurations of the isomers (*R* configuration for Rho A and *S* configuration for Rho B) at C4 in the oxazolidinone ring (ring 1 in the scheme). Furthermore, since the carbamic moiety of the oxazolidinone system (i.e., C4 in ring 1) bonds with H^+, Ca^{2+}, and Mg^{2+} ions, the structural parameters of the rhodostreptomycins are expected to change when they interact with these cations.

Molecular docking procedure

For the docking studies, Rho A and B were considered the targets and solvated or nonsolvated metallic ions the ligands. Nonpolar hydrogens were stripped away from Rho A and B using the AutoDock Tools 1.5.2 program [36], and the Mulliken charge on each whole system was calculated using the Gaussian program. When using the automated docking program AutoDock 4.0.1 [36], the interactions of Rho A/Rho B molecule with metal ions-water were considered rigid [36]. A 3-D grid box containing Rho A or B (30×30×30 Å) with a spacing of 0.375 Å was constructed. The Lamarckian genetic algorithm [36] was applied to search for Rho–metal interactions. All simulations were performed with an initial population of 100 randomly placed individuals and a maximum of 1×10^7 energy evaluations. The lowest-free-energy conformation was chosen. The other docking parameters were kept at the default values used by the AutoDock Tools 1.5.2 program [36]. Visualization of the protein–ligand complex was performed using Autodock Tools 1.5.2 [36] and Visual Molecular Dynamics (VMD) 1.8.6 [37].

Results and discussion

Geometrical and electronic parameters of Rho A and Rho B

The optimized geometrical data for Rho A and Rho B (Fig. 1) show that the calculated bond lengths in both molecules are very similar, except for the distance C2–N3, which appears to

Table 1 Bond angles (in degrees) in the oxazolidinone ring (ring 1) of Rho A and B, obtained using B3LYP/6-311G**

Angle	Rho A	Rho B	RhoA–H^+	RhoB–H^+	RhoA–Mg^{2+}	RhoB–Mg^{2+}	RhoA–Ca^{2+}	RhoB–Ca^{2+}
O2a–C2–N3	129.17	129.01	127.87	128.57	127.73	133.93	128.05	132.87
C2–N3–H	119.83	118.31	118.77	120.87	116.46	120.97	117.95	120.70
H–N3–C4	122.20	120.76	123.22	124.85	122.14	124.57	123.00	124.03
N3–C4–O4a	119.57	109.37	111.35	110.70	111.77	110.08	111.80	110.32

Table 2 Theoretical data on Rho A and B and their complexes, obtained using B3LYP/6-311G**

Molecule/complex	In the gas phase					In water as solvent				
	HOMO ($kcal mol^{-1}$)	LUMO ($kcal mol^{-1}$)	Dipole (D)	Hardness ($kcal mol^{-1}$)	ΔE ($kcal mol^{-1}$)	HOMO ($kcal mol^{-1}$)	LUMO ($kcal mol^{-1}$)	Dipole (D)	Hardness ($kcal mol^{-1}$)	ΔE ($kcal mol^{-1}$)
Rho A	−134.12	1.34	12.87	67.73	2.41	−144.92	9.17	10.07	77.05	2.50
Rho B	−144.20	5.12	7.60	74.66		−145.07	16.53	11.21	80.80	
Rho A–H^+	−186.64	−65.86	15.56	60.39	2.76	−146.09	1.61	19.36	73.85	11.20
Rho B–H^+	−191.53	−57.53	5.75	67.00		−147.20	−7.13	8.56	70.03	
Rho A–Mg^{2+}	−243.15	−156.19	24.32	43.48	24.30	−143.40	−25.90	30.68	58.75	9.93
Rho B–Mg^{2+}	−242.02	−163.76	7.52	39.13		−148.61	−27.25	7.52	60.68	
Rho A–Ca^{2+}	−238.43	−156.93	26.23	40.75	19.60	−143.59	−15.51	40.65	64.04	1.72
Rho B–Ca^{2+}	−239.93	−170.51	8.62	34.71		−148.01	−15.43	23.57	66.29	

be a double bond in Rho A (length 1.36 Å) and a single bond (length 1.37 Å) in Rho B. Results for bond angles were as follows: 119.83° in Rho A and 118.31° in Rho B for C2–N3–H, and 122.20° in Rho A and 120.76° in Rho B for H–N3–C4, meaning that small differences in these angles of 1.52° and 1.44° between Rho A and B were observed (see Table 1). Similarly, the bond angle of N3–C4–O4a was 119.57° in Rho A and 109.37° in Rho B (see Table 1); here, the carbon atom has different configurations for Rho A and B, and the difference in angle between Rho A and B is 10.2° (see Table 1). Furthermore, both Rho A and B are stabilized by hydrogen bonds (which range in length from 1.67 to 1.94 Å for Rho A and from 1.69 to 1.95 Å for Rho B; see Fig. 1). Total energy calculations for both isomers indicated that these systems are stable, given that ΔE is 2.50 $kcal mol^{-1}$ when they are solvated in water (see Table 2). The Mulliken population analyses revealed that the different types of reactive site, such as electrophilic and nucleophilic centers, are present (see Table 3). For example, for oxygen atoms values range from −0.335 to −0.398 and, in case of N3, values are −0.414, for Rho A, and −0.410, for Rho B, indicating that these atoms exhibit a nucleophilic character during the formation of a stable complex with a Ca^{2+} or Mg^{2+} ion.

Results for their electronic properties (see Table 2) show differences in chemical reactivity between Rho A and Rho B, and suggest that Rho B may be more reactive than Rho A when protonation occurs. For example, results for chemical hardness (η) show a slightly higher value for Rho B (74.66 $kcal mol^{-1}$) than for Rho A (67.73 $kcal mol^{-1}$), meaning that Ca^{2+} or Mg^{2+} can coordinate more effectively with Rho B than with Rho A. Results from molecular orbital studies showed that the HOMO orbital is localized over the nitrogen and oxygen of ring 1 (streptidine; see Scheme 1) for Rho A/B (see Fig. 2), suggesting that these atoms (N3a and O4a) may act as nucleophilic (Lewis base) sites in Rho A and Rho B that can interact with a cation (Lewis acid). Additionally, the HOMO-1 orbital was detected 0.02 eV (for Rho A) and 0.01 eV (for Rho B) below the HOMO, indicating that the nitrogen atoms (guanidine) of the α-L-streptose (ring 4) contribute to the *p*- and π-orbital character of the C–N and N=C bonds. Furthermore, the small energy difference between the HOMO and HOMO-1 orbitals favors the formation of a stable complex with a Ca^{2+} or Mg^{2+} ion.

Geometrical and electronic parameters of Rho A–H^+ and Rho B–H^+

Regarding interactions between Rho A/B and an H^+ ion, it was observed that there were many possible modes of

Table 3 Mulliken charges for certain nitrogen, oxygen, and carbon atoms in Rho A and B and their complexes, obtained using B3LYP/6-311G **

Atom	Rho A	Rho B	Rho A–H^+	Rho B–H^+	Rho A–Ca^{2+}	Rho B–Ca^{2+}	Rho A–Mg^{2+}	Rho B–Mg^{2+}
O1	−0.335	−0.343	−0.306	−0.328	−0.305	−0.439	−0.297	−0.447
O2a	−0.370	−0.342	−0.310	−0.291	−0.273	−0.260	−0.254	−0.236
O4a	−0.398	−0.398	−0.486	−0.426	−0.543	−0.568	−0.563	−0.556
N3	−0.414	−0.410	−0.449	−0.416	−0.462	−0.356	−0.456	−0.346
C2	0.485	0.464	0.485	0.481	0.494	0.456	0.484	0.491
C4	0.263	0.257	0.334	0.322	0.326	0.269	0.336	0.287
C5	−0.098	−0.08	−0.145	−0.100	−0.097	−0.186	−0.085	−0.186
H^+, Ca^{2+}, Mg^{2+}			0.389	0.372	1.307	1.350	1.016	1.030

interaction. However, electrostatic potential maps indicated that ring 1 has the highest electron density (see Fig. 3). For this reason, we only simulated protonation on the oxazolidinone ring. The optimized geometries of Rho A–H^+ and Rho B–H^+ were calculated using B3LYP/6-311G** (see Fig. 4), and the results indicated that the geometrical parameters for ring 1 (streptidine) changed considerably upon the protonation of Rho A to Rho A–H^+, mainly due to the increased length of the C4–O4a bond, which stretched from 1.40 Å to 1.45 Å [19]. However, although there was no significant difference in bond length between the neutral and protonated structures of Rho B, a small difference was observed in the bond angles of the oxazolidinonic moiety (ring 1, streptidine); see Table 1.

Mulliken charge analysis (see Table 3) showed that heteroatoms such as oxygen possessed higher charge densities (ranging from −0.291 to −0.486 and from −0.449, for N3–Rho A–H^+, to −0.416, for N3–Rho B–H^+) than other atoms (see Fig. 5). Furthermore, it was observed that the electron density of O2a decreased from −0.370 to −0.310, and that of N3 increased from −0.414 to −0.449, when the neutral structure was protonated to Rho A–H^+. The same behavior was

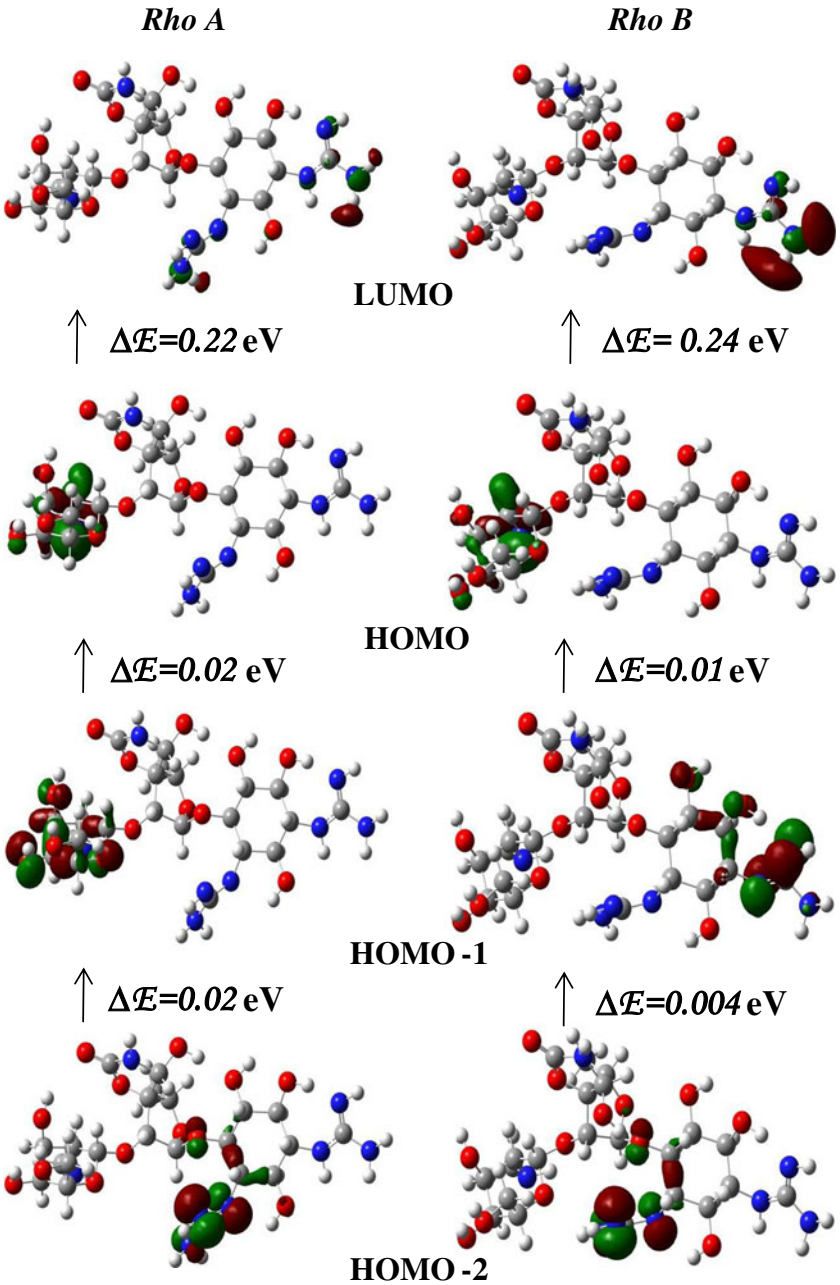

Fig. 2 HOMO, HOMO-1, and HOMO-2 (shown in 3D) orbitals for molecules Rho A and Rho B, obtained using B3LYP/6-311G **

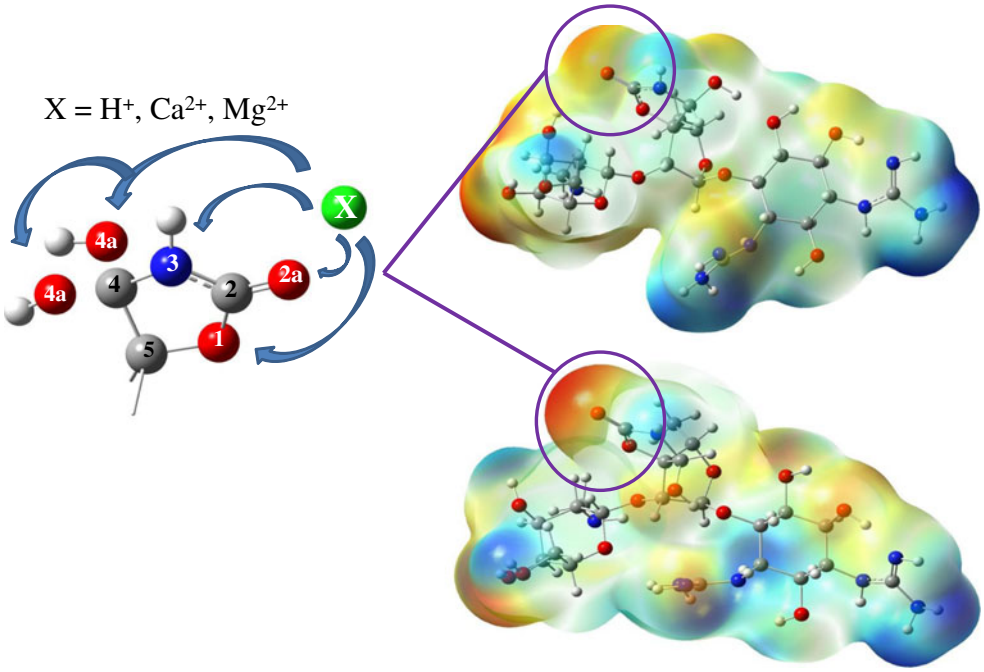

Fig. 3 Inferred mechanism of the interaction of an ion with the active sites of Rho A and Rho B

observed when the neutral structure of Rho B was protonated to Rho B–H^+ (the electron density of O1 decreased from −0.343 to −0.328 and that of O2a decreased from −0.342 to −0.291). According to the results for Mulliken charges (see Fig. 5), the oxazolidinone ring (ring 1, streptidine) was further stabilized by the protonation of either Rho A or Rho B. From the results of molecular orbital studies on the protonated structures, it was observed that the HOMO was localized over N3a of the L-aminoglucoside ring (ring 3, α-L-glucosamine; see Scheme 1), and it was *p* type in nature (see Fig. 6), exhibiting small π-orbital contributions from various oxygen atoms (O4a, O5a). Similarly, for Rho B–H^+, the HOMO over N3, O4a, and O5a of ring 3 (α-L-glucosamine) is *p* type in nature. The HOMO-1 molecular orbital that was needed to achieve a bond with σ and π character was localized over oxygens 4a and 5a in ring 3 (α-L-glucosamine) in the Rho A–H^+ systems. The results show the contribution from the homocyclic ring 4 (α-L-streptose) to the molecular orbital of the guanidine group in the case of Rho B–H^+.

Hydrogen bonds were present in the protonated structures that were optimized; for example, there were two H-bonds (O5a–H···O7a, 1.90 Å, ring 3; and O6a–H···OO5a, 1.73 Å, ring 4) that stabilized the Rho A–H^+ structure and one hydrogen bond in Rho B–H^+ (O5a–H···O5a, 1.61 Å, ring 4; see Fig. 4). After analyzing data on the total energies of the protonated structures, it was found that Rho B–H^+ is more stable than Rho A–H^+, with an energy difference of 2.76 kcal mol^{-1} in the gas phase (see Table 2). This result is in accord with experimental observations [1], which suggest that protonated Rho B is stabilized in a similar way to the mechanism of a proton pump inhibitor, which is a characteristic of drugs that act to reduce the production of gastric acid and neutralize the ionic activity in the medium [38].

Abilities of Rho A and Rho B to coordinate with Ca^{2+} or Mg^{2+}

The abilities of Rho A and B to coordinate with Ca^{2+} or Mg^{2+} were analyzed using theoretical methods (see Fig. 3). The addition of Ca^{2+} to oxazolidinone (ring 1) was performed by total relaxation, and the lowest energy was obtained for Rho A–Ca^{2+} when Ca^{2+} was bonded to O4a, O7 (rings 1 and 2), O6a (ring 4), and O8a. Similarly, Rho B–Ca^{2+} was found to be most stable when Ca^{2+} coordinated with O1, O4a (rings 1 and 2), O1, and O7a (ring 3) of Rho B. Likewise, the coordination behavior of Rho A or Rho B with Mg^{2+} was analyzed. The optimized geometries (of Rho A–Ca^{2+}, Rho B–Ca^{2+}, Rho A–Mg^{2+}, and Rho B–Mg^{2+}) were calculated using B3LYP/6-311G** (see Figs. 7 and 8), and these results showed that there was no significant difference in the bond lengths obtained when either Ca^{2+} or Mg^{2+} coordinated with L-aminoglucoside: O4a–Ca^{2+} = 2.38 Å for Rho A–Ca^{2+} and 2.33 Å for Rho B–Ca^{2+} (see Fig. 7). Additionally, slight changes in the bond angles O2a–C2–N3, C2–N3–H, H–N3–C4, and N3–C4–O4a in the oxazolidinone ring (ring 1) were observed after its coordination with Ca^{2+} or Mg^{2+}; see Table 1. The angle O2a–C2–N3 showed differences of 6.2° between Rho A–Mg^{2+} and Rho B–Mg^{2+} and 4.82° between Rho A–Ca^{2+} and Rho B–Ca^{2+}. Furthermore, bond delocalization over

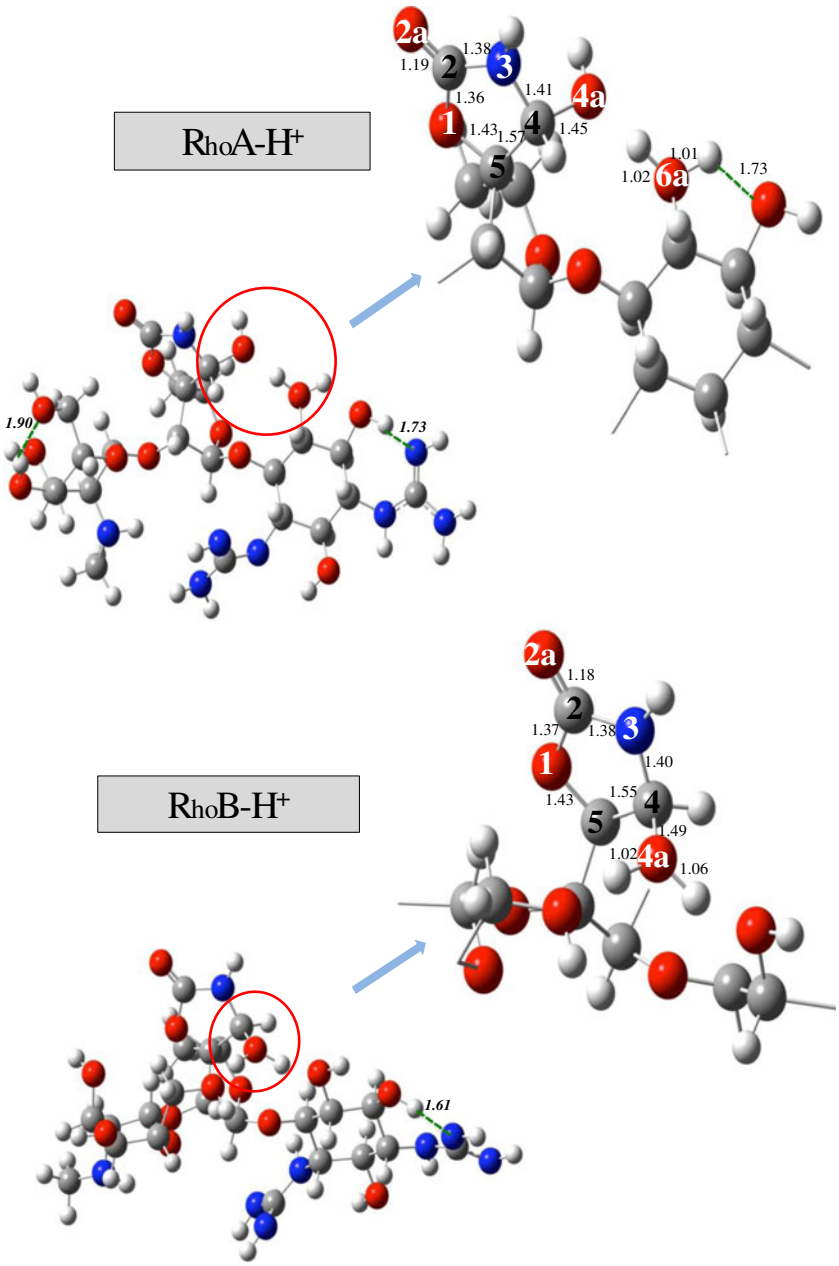

Fig. 4 Optimized geometries (shown in 3D) of Rho A–H^+ and Rho B–H^+, as calculated with B3LYP/6-311G**. Some bond lengths (in Å) in the oxazolidinone ring (ring 1) are shown, at the site that undergoes protonation, and bridging hydrogen bonds that are present during the protonation of the system are also depicted

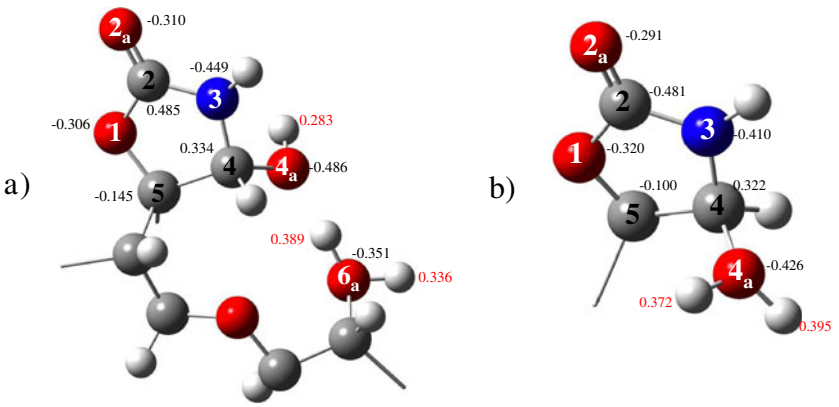

Fig. 5 Mulliken charges (shown in 3D) for the amine site of the Rho A–H^+ (**a**) and Rho B–H^+ (**b**) using B3LYP/6-311G **

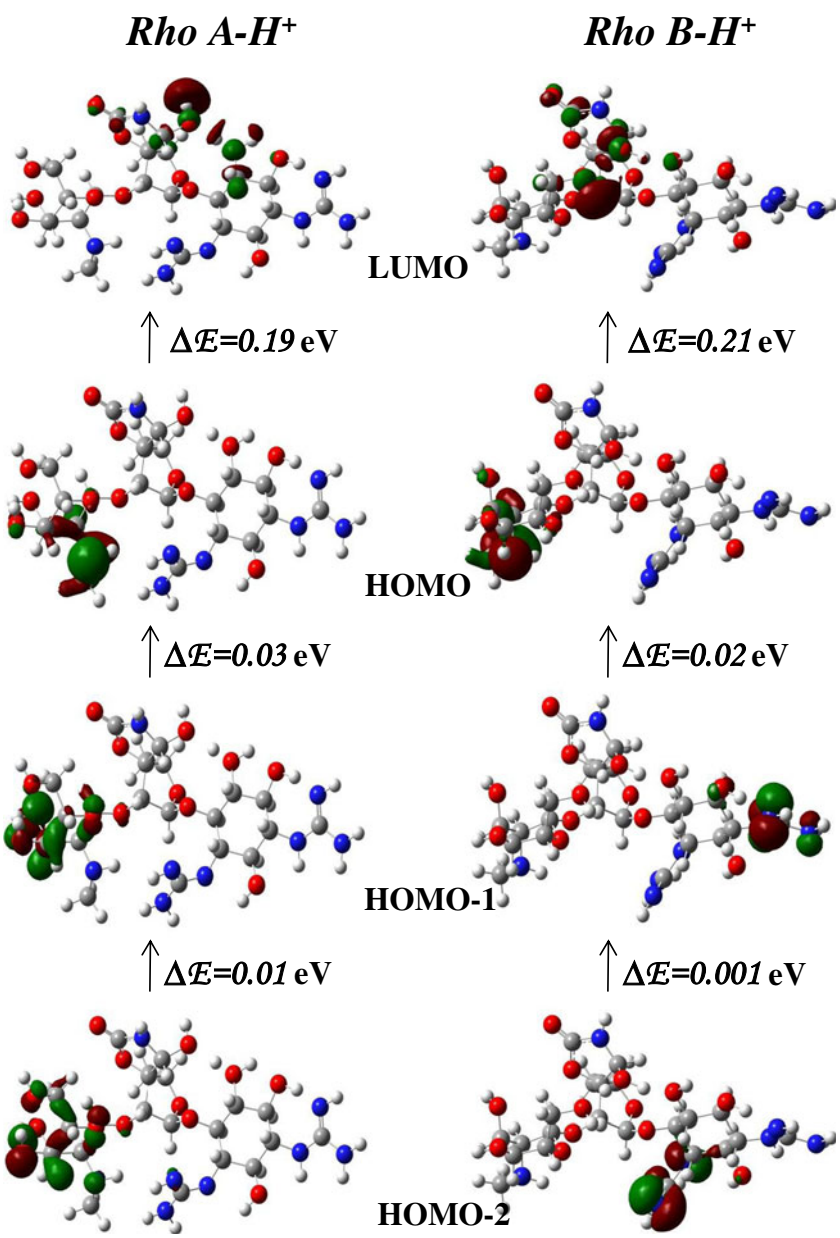

Fig. 6 HOMO, HOMO-1, and HOMO-2 (shown in 3D), molecules of Rho A–H^+ and Rho B–H^+ using B3LYP/6-311G **

the nitrogen of the guanidine group (homocyclic ring 4) of Rho A–Ca^{2+} was noted (see Fig. 9), and O and Ca^{2+} were observed to coordinate. This led to system stabilization, as the four atoms O4a, O7 (ring 1), O6a (ring 4), and O8a coordinated to Ca^{2+} at distances of 2.38, 2.37, 2.07, and 2.53 in this system. Similarly, for Rho B–Ca^{2+}, there was coordination between Ca^{2+} and the four atoms O1, O4a (ring 1), O1, and O7a (ring 3) at distances of 2.50, 2.33, 2.30, and 2.28, respectively. For Rho A–Mg^{2+}, the three atoms O4a, O7 (rings 1 and 2), and O6a (ring 4) were seen to coordinate with Mg^{2+} at distances of 2.03, 2.08, and 1.86 Å; for Rho B–Mg^{2+}, the Mg^{2+} coordinated to O4a (ring 1), O1, and O7a (ring 3) at distances of 2.02, 2.02, and 1.98 Å. In the case of Mg^{2+} with Rho B, the oxazolidinone ring (N3–C2 and C2–O2a) forms a delocalized region, whereas the equivalent region in Rho A–Mg^{2+} is the guanidine of ring 4 (see Fig. 8).

Mulliken charge analysis (see Table 3) showed that the oxazolidinone ring (ring 1) donates charge to Ca^{2+}; for example, O4a increased in charge density from −0.398 to −0.568 after the coordination of Rho A to Ca^{2+}, whereas O2a dropped in charge density from −0.370 to −0.273; similarly, the charge density on O2a decreased from −0.370 from −0.260 when Rho B coordinated with Ca^{2+}, whereas N3 gained charge (changing from −0.414 to −0.462), but C4 lost charge (changing from 0.263 to 0.326 on average). However, in this case, the Ca^{2+} ion increased in charge density by around 0.7 electrons (see Fig. 10). These

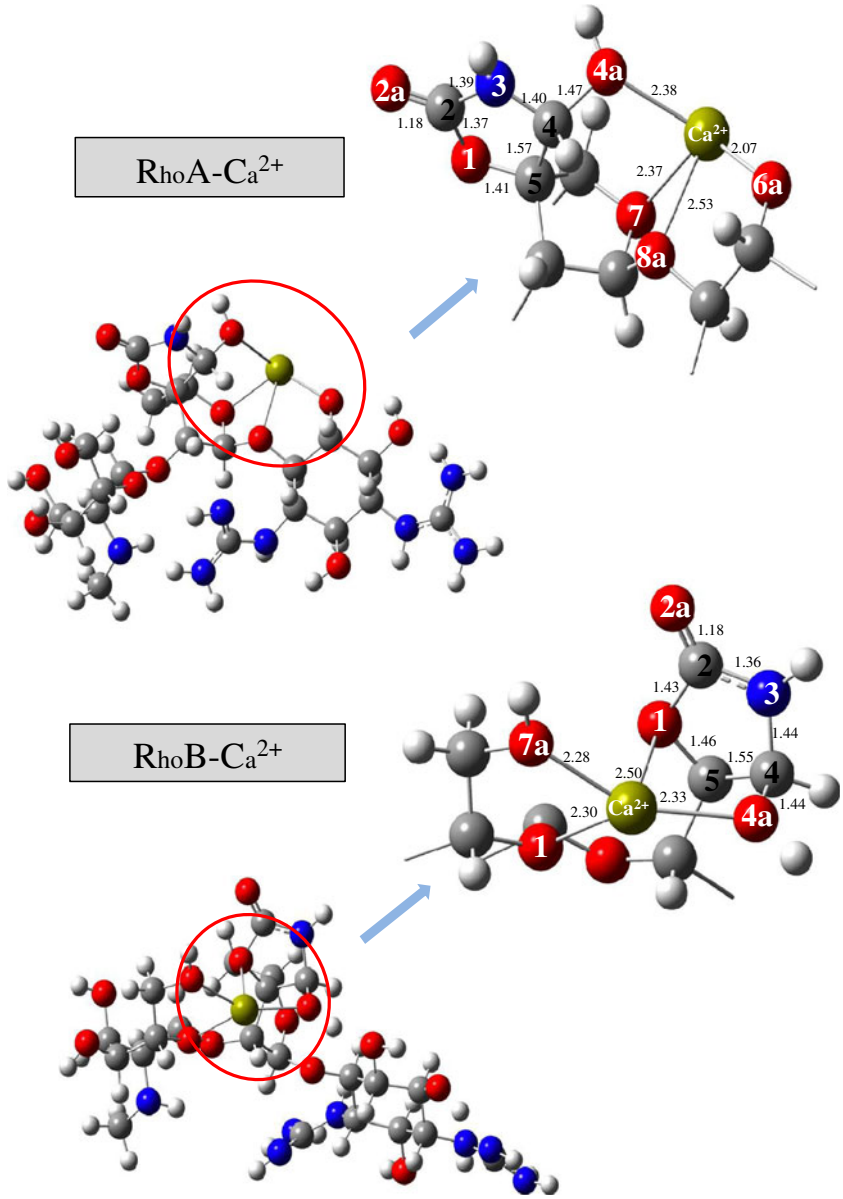

Fig. 7 Optimized geometries (shown in 3D) of Rho A–Ca^{2+} and Rho B–Ca^{2+}, as calculated with B3LYP/6-311G**. Some bond lengths (in Å) in the oxazolidinone ring (ring 1) are shown, as well as the coordination towards Ca^{2+}

values agree with the bond lengths in the L-aminoglucoside ring (ring 1), and the Mulliken charges for the Mg^{2+} complex were found to be similar to those for the Ca^{2+} complex.

The total energy results indicated that Rho A–Ca^{2+} is more energetically stable than Rho B–Ca^{2+}, with a difference of 1.72 kcalmol^{-1} in water as a solvent. Similar results were obtained for Mg^{2+} with Rho (in this case, the difference in energy was 9.93 kcalmol^{-1} in water as a solvent; see Table 2). This difference may be due to the considerable strength of the O–Ca and N–Ca bonds [39] and the formation of other H-bonds. Therefore, the binding energy (BE) was calculated using the following equations:

$$BE = E_{RhoA-Ca^{2+}} - [E_{RhoA} + E_{Ca^{2+}}] \quad (I.1)$$

$$BE = E_{RhoB-Ca^{2+}} - [E_{RhoB} + E_{Ca^{2+}}] \quad (I.2)$$

$$BE = E_{RhoA-Mg^{2+}} - [E_{RhoA} + E_{Mg^{2+}}] \quad (I.3)$$

$$BE = E_{RhoB-Mg^{2+}} - [E_{RhoB} + E_{Mg^{2+}}]. \quad (I.4)$$

Binding energy data predict that Rho A forms a more stable complex than Rho B does with Ca^{2+} or Mg^{2+} (see Table 4). For example, the binding energies for the unhydrated complexes were −223.67 (Rho A–Ca^{2+}), −207.59 (Rho B–Ca^{2+}), −300.46 (Rho A–Mg^{2+}), and −280.05 (Rho B–Mg^{2+}) kcalmol^{-1}.

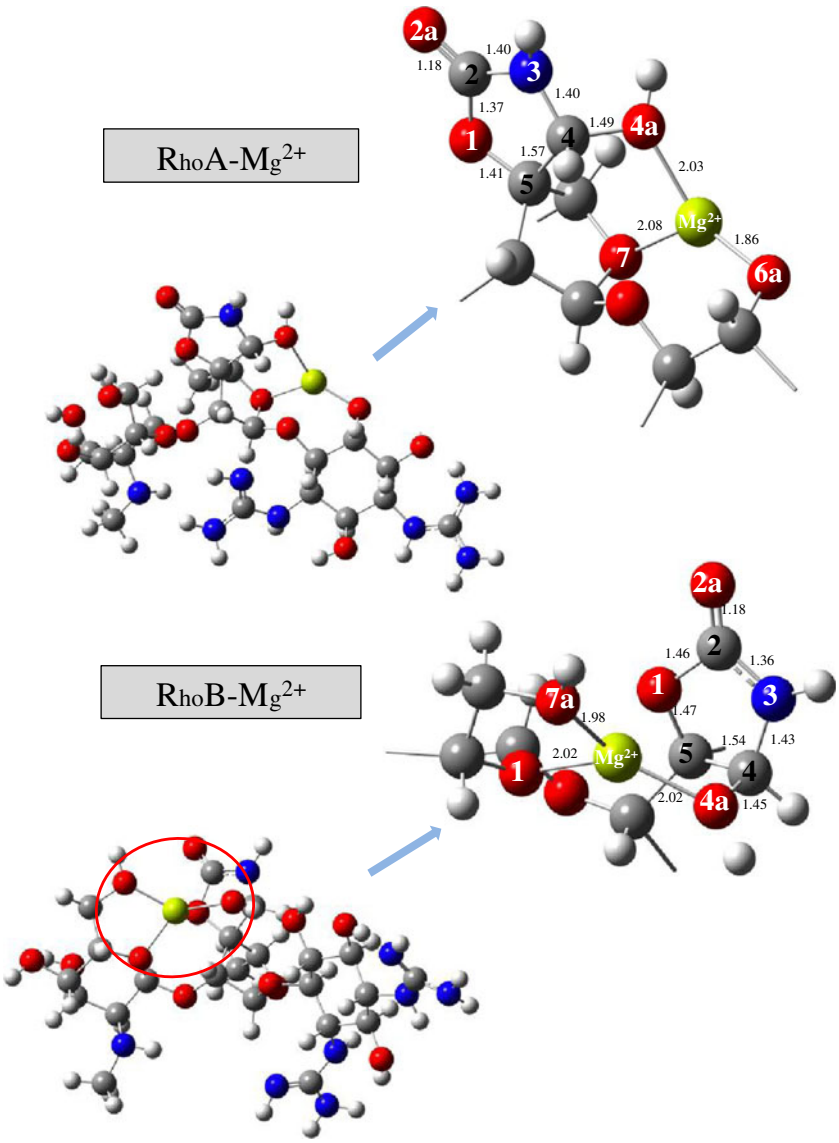

Fig. 8 Optimized geometries (shown in 3D) of Rho A–Mg^{2+} and Rho B–Mg^{2+}, as calculated with B3LYP/6-311G**. Some bond lengths (in Å) in the oxazolidinone ring (ring 1) are shown, as well as the coordination towards Mg^{2+}

Docking studies

With the aim of analyzing nonbonded interactions by exploring the most favorable contact of the Rho A or B surface with Ca^{2+} or Mg^{2+}, a docking procedure that considered the explicit coordination of water molecules with metal ions was implemented [28]. The docking procedure was also performed for the unhydrated ions. Since metal ions are solvated in an aqueous environment [40], they can interact with solvated target molecules [41]. We therefore explored the interactions of the solvated metals ions with Rho A or B (see Fig. 11), and found that the hydrogen-bonding network within the stereoisomer governs the interaction with Mg^{2+} or Ca^{2+}. Furthermore, water molecules act as hydrogen donators and oxygen and nitrogen atoms in the Rho molecules can act as hydrogen acceptors. Also, the oxygen atom in a water molecule can act as a hydrogen acceptor and the guanidinic group (N3) of Rho A can act as a hydrogen donator. The bonds between metal and water show that oxygen atoms facilitate interactions through molecular coordination [42] during the docking

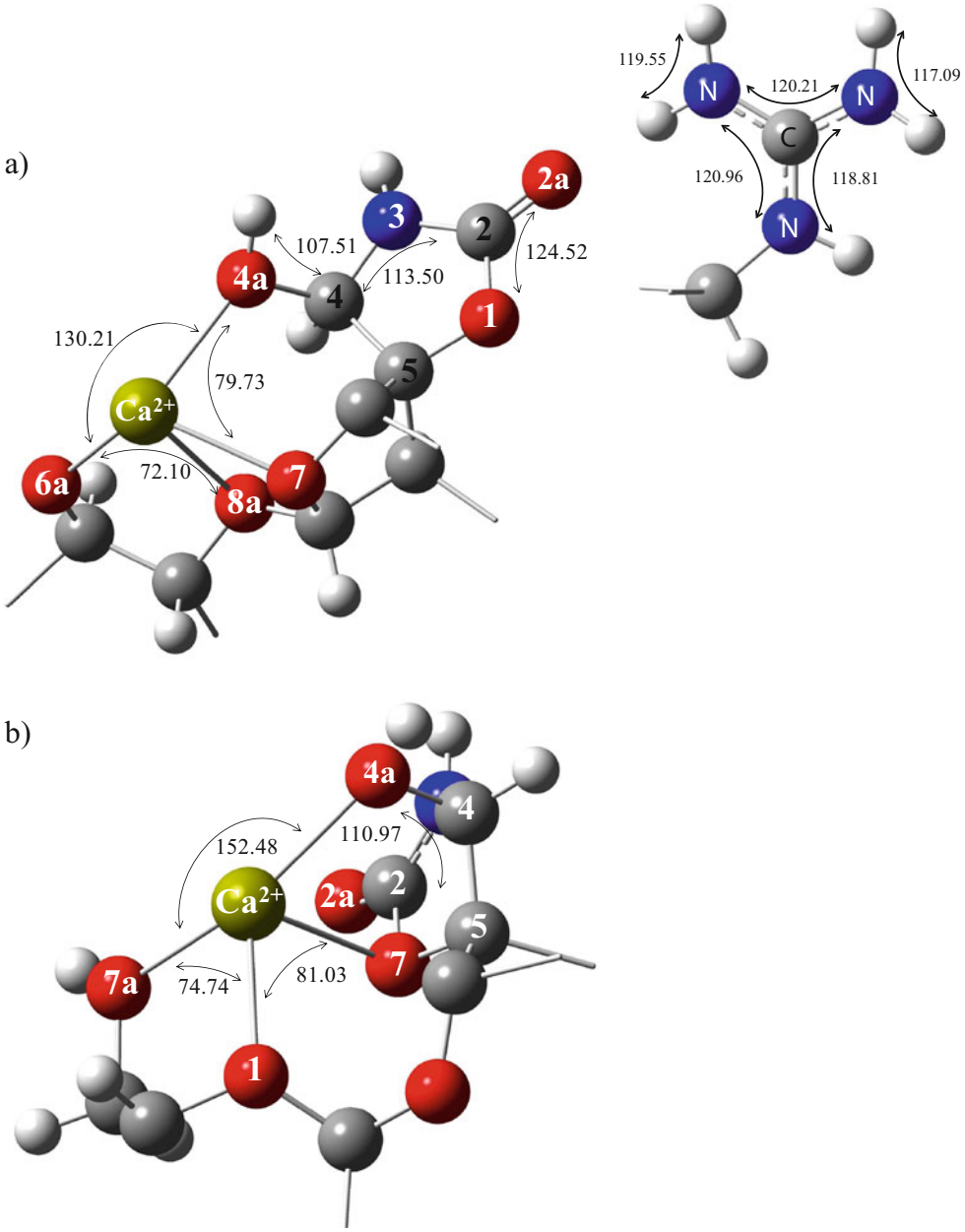

Fig. 9 Bond angles (shown in 3D), in degrees, that occur during the interaction of either (**a**) Rho A or (**b**) Rho B with Ca^{2+}, and the angles seen at the site of the amines on ring 4 of the Rho A–Ca^{2+} complex

studies all water molecules were maintained despite of being free or non-bonded. Solvated metal ions recognizes small ligands, as also happens with tetracyclines [43]. When metal ion–water complexes were present (see Fig. 11), the water molecules were arranged in such a way that they formed some hydrogen bonds with Rho A or Rho B while the metal ion was located in the cavity of Rho (see Fig. 11).

RhoA–$Ca^{2+}(H_2O)_6$ is stabilized by the following interactions: H···O7a = 1.725 Å, H···O1(ring 3) = 1.766 Å, H···O3a = 1.720 Å, H···N3 = 2.085 Å, H···N(a) = 1.972 Å, and H···N(e) = 1.634 Å. RhoA–$Mg^{2+}(H_2O)_6$ is stabilized by the following interactions: H···O7a = 1.713 Å, H···O1 (ring 3) = 1.785 Å, H···O3a = 1.731 Å, H···N3 = 2.121 Å, H···N(a) = 1.971 Å, and H···N(e) = 1.602 Å. In addition, RhoB–$Ca^{2+}(H_2O)_6$ is stabilized by the following interactions: H···O8a = 1.985 Å, H···O1(ring 3) = 1.774 Å, H···O3a = 1.827 Å, H···N(a) = 1.791 Å, and two H···N(e)···H = 1.649–1.888 Å interactions, while RhoB–$Mg^{2+}(H_2O)_6$ is stabilized by H···O7a = 1.759 Å, H···O6a = 1.745 Å, H···N(b) = 1.623 Å, H···N(e) = 1.687 Å, and two H···O(ring 3)···H = 1.758–1.936

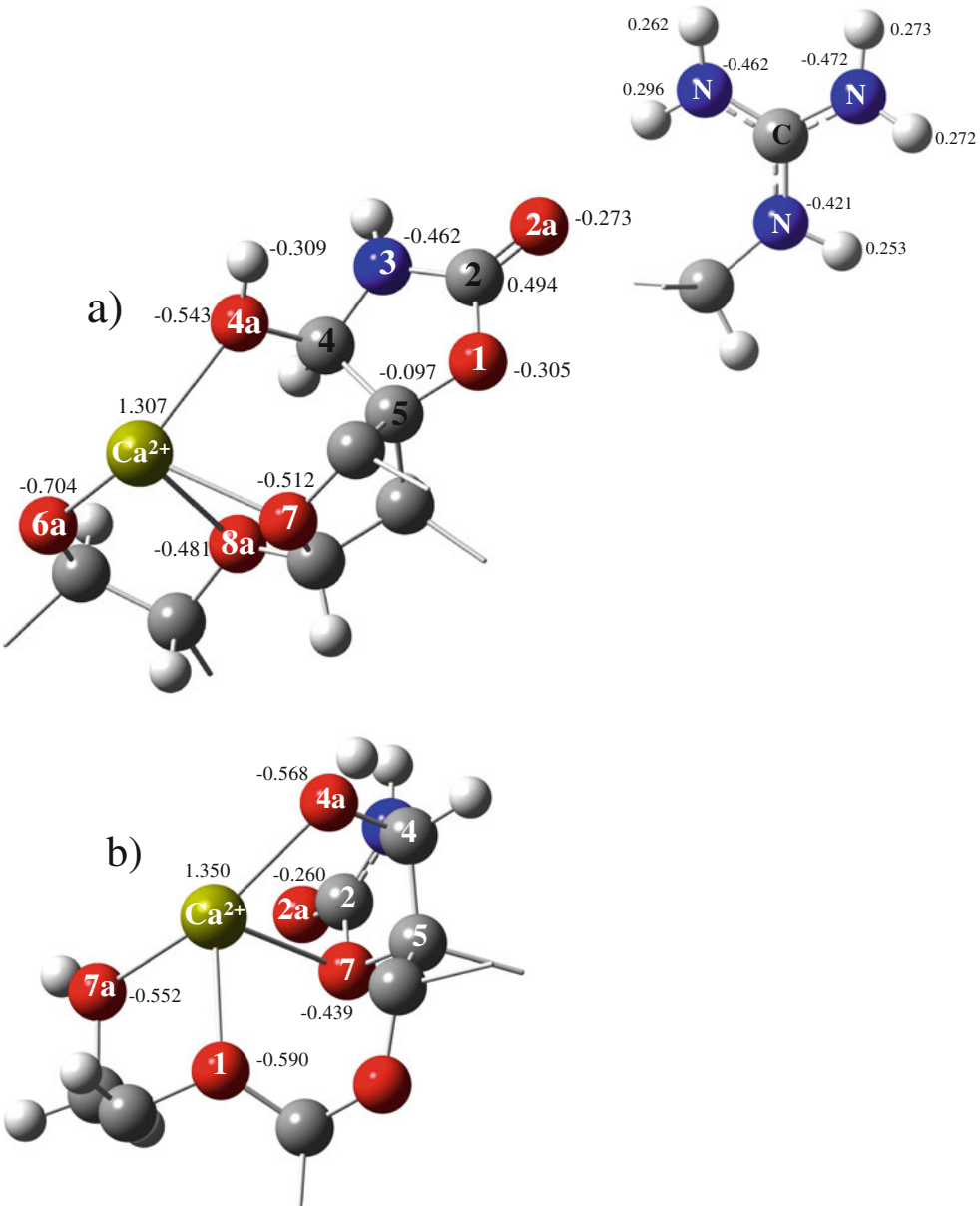

Fig. 10 Some Mulliken charges (shown in 3D) in the (**a**) Rho A–Ca^{2+} and (**b**) Rho B–Ca^{2+} complexes, as calculated using B3LYP/6-311G**

Table 4 Relevant energies for (hydrated and unhydrated) complexes of Rho A or Rho B with Ca^{2+} or Mg^{2+}, calculated using B3LYP/6-311G**

Complex	BE (kcalmol^{-1})	ΔH (kcalmol^{-1})	ΔS (kcalmol^{-1} K)
Rho A–Ca^{2+}	−223.67	−224.42	0.26
Rho B–Ca^{2+}	−207.59	−208.69	0.26
Rho A–Mg^{2+}	−300.46	−301.56	0.25
Rho B–Mg^{2+}	−280.05	−281.49	0.25
Rho A–Ca^{2+} $(H_2O)_6$	−70.18	−72.21	0.33
Rho B–Ca^{2+} $(H_2O)_6$	−70.54	−72.53	0.32
Rho A–Mg^{2+} $(H_2O)_6$	−71.80	−72.99	0.32
Rho B–Mg^{2+} $(H_2O)_6$	−93.68	−95.00	0.32

Å hydrogen bonds. These intermolecular hydrogen bonds between the Rho structure and a cation are strong.

Rho B forms the lowest energy (most stable) metal complex with Mg^{2+} (see Table 4): Rho B–$Mg^{2+}(H_2O)_6$ (−93.68 kcal mol^{-1}). This could be due to cationic and stereoisomeric effects, as well as the presence of water molecules, which induce stronger repulsive effects than those afforded by hydrogen interactions. In this work, there is less interaction between hydrated calcium and Rho B, while the interaction between Rho B and calcium ions without hydration is very strong, this due to the characteristics of the cation. Accordingly, it is also important to consider the type of Rho stereoisomer involved. The Rho B–$Mg^{2+}(H_2O)_6$ complex shows fewer intermolecular

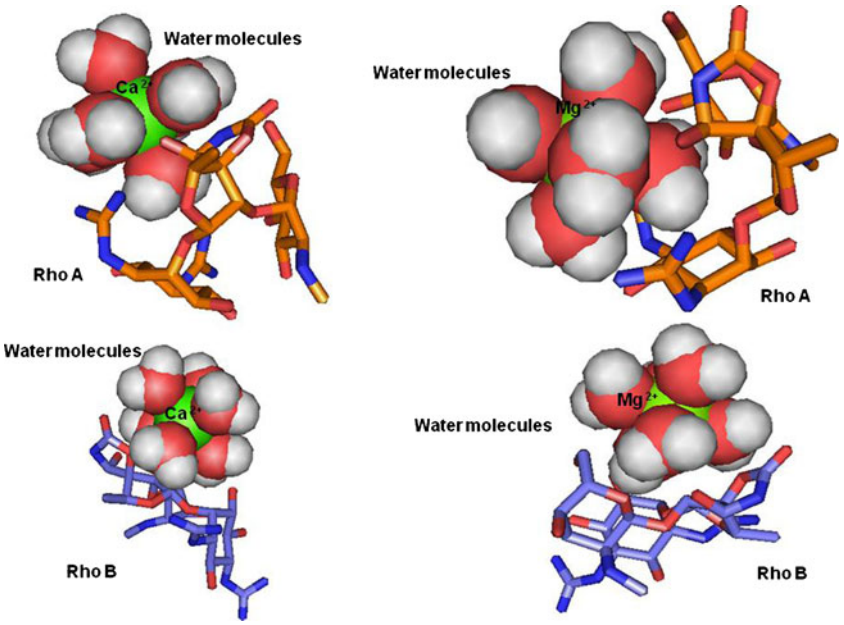

Fig. 11 Interactions of solvated metal ions with Rho molecules

interactions than the Rho A–$Mg^{2+}(H_2O)_6$ complex, and some of the hydrogen-bond distances are shorter in the latter complex. The hydrated Ca^{2+} ion had the lowest affinity with Rho A, followed by the Rho B–Ca^{2+} complex.

Thermochemical values calculated with B3LYP/6-311G** for these complexes showed a high affinity of the Mg^{2+} cation hydrated with Rho B. Hence, for Rho A–$Ca^{2+}(H_2O)_6$, ΔH = −72.21 kcal mol^{-1} for Rho B–$Ca^{2+}(H_2O)_6$ ΔH = −72.53 kcal mol^{-1} for Rho A–$Mg^{2+}(H_2O)_6$ ΔH = −72.99 kcal mol^{-1}, and for Rho B–$Mg^{2+}(H_2O)_6$ ΔH = −95.00 kcal mol^{-1}, confirming that Rho B binds most strongly to the hydrated Mg^{2+} ion (Table 4). This result agrees with experimental observations [1].

Conclusions

After a total energy comparison, it was observed that protonated Rho B is more stable than protonated Rho A. There is a difference of 2.76 kcal mol^{-1} between these two systems, based on the energy needed to form the two hydrogen bonds that stabilize each system. This result agrees with reported experimental results which indicate that Rho B causes greater bacterial growth inhibition than Rho A, because in acid medium, Rho B is protonated better than Rho A, Rho B–H^+ showed higher stability since it is considered a proton pump inhibitor, and is therefore a stronger inhibitor of *Helicobacter pylori*. Similarly, the calculated thermochemical values for these complexes showed that its high affinity for Mg^{2+} cause the hydration of RhoB: for Rho A–$Ca^{2+}(H_2O)_6$, ΔH = −72.21 kcal mol^{-1} for Rho B–$Ca^{2+}(H_2O)_6$ ΔH = −72.53 kcal mol^{-1} for Rho A–$Mg^{2+}(H_2O)_6$ ΔH = −72.99 kcal mol^{-1} and for Rho B–$Mg^{2+}(H_2O)_6$ ΔH = −95.00 kcal mol^{-1}, confirming that the Rho B molecule binds most strongly with the hydrated Mg^{2+} ion. Water molecules may play an important role in interactions between Rho A or B and Ca^{2+} or Mg^{2+}. Some small molecules induce their biological activity reaching their receptor (protein) binding sites through hydrogen bonding, acting as a mediator of water molecules, and possibly explaining the role of the hydrated cation.

Acknowledgments Their access to the KanBalam supercomputer at Dirección General de Cómputo y de Tecnologías de Información y Comunicación (DGTIC-UNAM) is greatly appreciated by the authors. Secretaria de Investigación y Posgrado, Comisión de Operación y Fomento de Actividades del Instituto Politécnicos Nacional, Consejo Nacional de Ciencia y Tecnología (CONACYT) y Instituto de Ciencia y Tecnología del Distrito Federal (ICyTDF).

References

1. Kurosawa K, Ghiviriga I, Sambandan TG, Lessard PA, Barbara JE, Rha C, Sinskey AJ (2008) Rhodostreptomycins, antibiotics biosynthesized following horizontal gene transfer from *Streptomyces padanus* to *Rhodococcus fascians*. J Am Chem Soc 130:1126–1127
2. Edwards BK, Ward E, Kohler BA, Eheman C, Zauber AG, Anderson RN, Jemal A, Schymura MJ, Lansdorp-Vogelaar I, Seeff LC, van Ballegooijen M, Goede SL, Ries LAG (2010) Annual report to the nation on the status of cancer, 1975–2006, featuring colorectal cancer trends and impact of interventions (risk factors, screening, and treatment) to reduce future rates. Cancer 116:544–573
3. Dutch DS, Gary SK (2003) Biosynthesis and functioning of tetrahydrobiopterin. J Nutr Biochem 2:411–423
4. Tillman JA, Seybold SJ, Jurenka RA, Blomquist GA (1999) Insect pheromones—an overview of biosynthesis and endocrine regulation. Insect Biochem Mol Biol 29:481–514
5. Pirrung MC, Cao J, Chen J (1998) Ethylene biosynthesis: processing of a substrate analog supports a radical mechanism for the ethylene-forming enzyme. Chem Biol 5:49–57

6. Piaggesia A, Picciarellia P, Ceccarellia N, Lorenzi R (1998) Cytokinin biosynthesis in endosperm of *Sechium edule* Sw. Plant Sci 129:131–140
7. Kamiya Y, García-Martínez JL (1999) Regulation of gibberellin biosynthesis by light. Curr Opin Plant Biol 2:398–403
8. Nora GP, Miller MJ, Möllmann U (2006) The synthesis and in vitro testing of structurally novel antibiotics derived from acylnitroso Diels–Alder adducts. Bioorg Med Chem Lett 16:3966–3970
9. Kennedy AD, DeLeo FR (2009) Epidemiology and virulence of community-associated MRSA. Clin Microbiol Newsl 31:153–160
10. Lafuente RF, Rosell CM, Piatkowska B, Guisán JM (1995) Synthesis of antibiotics (cephaloglycin) catalyzed by penicillin G acylase: evaluation and optimization of different synthetic approaches. Enz Microb Technol 17:517–523
11. Herrero IA, Teshager T, Garde J, Moreno MA, Domínguez L (2000) Prevalence of vancomycin-resistant *Enterococcus faecium* (VREF) in pig faeces from slaughterhouses in Spain. Prev Vet Med 47:255–262
12. Habeck M (2002) Spying on nature's drug factories. Drug Discovery Today 7:1109–1110
13. Hutchinson CR (1998) Combinatorial biosynthesis for new drug discovery. Curr Opin Microbiol 1:319–329
14. Foubister V (2003) Scientists expand the genetic code drug discovery. Today 8:239–840
15. Andersson C, Lönnroth C, Moldawer LL, Ternell M, Lundholm K (1990) Increased degradation of albumin in cancer is not due to conformational or chemical modifications in the albumin molecule. J Surg Res 49:23–29
16. Sitaram N, Subbalakshmi C, Nagaraj R (2003) A 13-residue basic antimicrobial peptide rich in tryptophan and proline interacts with Ca^{2+}-calmodulin. Biochem Biophys Res Commun 309:879–884
17. Kwon HJ, Lee GY (2008) A DFT study on magnesium ion affinity of glycine. J Korean Chem Society 52:207–211
18. Rasul R, Cole N, Balasubramanian D, Chen R, Kumar N, Willcox P (2010) Interaction of the antimicrobial peptide melimine with bacterial membranes. Int J Antimicrob Agents 35:566–572
19. Lin T-S, Fishman E (1967) Enthalpies of intramolecular hydrogen bonds of orthohalophenols and deuterated orthohalophenols in the vapor phase. Spectrochim Acta Part A 23:491–500
20. Shoyele SA, Cawthorne S (2006) Particle engineering techniques for inhaled biopharmaceuticals. Adv Drug Deliv Rev 58:1009–1029
21. Walsh G (2004) Second-generation biopharmaceuticals. Eur J Pharm Biopharm 58:185–196
22. Loria CJ, Echeverria P, Smith AL (1976) Effect of antibiotic formulations in serum protein: bilirubin interaction of newborn infants. J Pediatr 89:479–482
23. Nogimori K, Tamura M, Yajima M, Ito K, Nakamura T, Kajikawa N, Maruyama Y, Ui M (1984) Dual mechanisms involved in development of diverse biological activities of islet-activating protein, pertussis toxin, as revealed by chemical modification of lysine residues in the toxin molecule. Biochim Biophy Acta 801:232–243
24. Yamniuk AP, Vogel HJ (2005) Calcium and magnesium-dependent interactions between calcium- and integrin-binding protein and the integrin αIIb cytoplasmic domain. Protein Sci 14:1429–1437
25. Chan KW, Wu Y, Liu ZF (2008) Solvation effects on the intracluster elimination channels in M+(L)n, where M^+ = Mg+ and Ca+, L = CH_3OH, and NH_3, and n = 2–6). J Phys Chem A 112:8542–8550
26. Martin-Garcia JM, Ruiz-Sanz J, Luque I (2012) Interfacial water molecules in SH_3 interactions: a revised paradigm for polyproline recognition. Biochem J 442:443–451
27. Gresh N, De Courcy B, Piquemal JP, Foret J, Courtiol-Legourd S, Salmon L (2011) Polarizable water networks in ligand-metalloprotein recognition. Impact on the relative complexation energies of Zn-dependent phosphomannose isomerase with D-mannose 6-phosphate surrogates. J Phys Chem B 115:8304–8316
28. Samsonov SA, Teyra J, Pisabarro MT (2011) Docking glycosaminoglycans to proteins: analysis of solvent inclusion. J Comput Aided Mol Des 25:477–489
29. Frisch MJ et al (2011) GAUSSIAN 09, revision B.01. Gaussian Inc., Wallingford
30. Lee C, Yang W, Parr RG (1988) Development of the Colle–Salvetti correlation-energy formula into a functional of the electron density. Phy Rev B 37:785–789
31. Miehlich B, Savin A, Stoll H, Preuss H (1989) Results obtained with the correlation-energy density functionals of Becke and Lee, Yang and Parr. Chem Phys Lett 157:200–206
32. Becke AD (1988) Density-functional exchange-energy approximation with correct asymptotic behavior. Phys Rev A 38:3098–3100
33. Courcy B, Pedersen LG, Parisel O, Gresh N, Silvi B, Pilmé J, Piquemal JP (2010) Understanding selectivity of hard and soft metal cations within biological systems using the subvalence concept. 1. Application to blood coagulation: direct cation–protein electronic effects versus indirect interactions through water networks. J Chem Theory Comput 6:1048
34. Tomasi J, Mennucci B, Cammi R (2005) Quantum mechanical continuum solvation models. Chem Rev 105:2999–3093
35. Kahn RS, Ingold CK, Prelog V (1956) The specification of asymmetric configuration in organic chemistry. Experientia 12:81–94
36. Morris GM, Goodsell DS, Halliday RS, Huey R, Hart WE, Belew RK, Olson AJ (1998) Automated docking using a Lamarckian genetic algorithm and an empirical binding free energy function. J Comput Chem 19:1639–1662
37. Humphrey W, Dalke A, Schulten K (1996) VMD: visual molecular dynamics. J Mol Graphics 14:33–38
38. Han D, Namslauer A, Pawate A, Morgan JE, Nagy S, Vakkasoglu AS, Brzezinski P, Gennis RB (2006) Replacing asn207 by aspartate at the neck of the D channel in the aa 3 type cytochrome c oxidase from *Rhodobacter sphaeroides* results in decoupling the proton pump. Biochemistry 45:14064–14074
39. Kirschner KN, Bowen B, Ma JP, Duncan MA (1998) Theoretical investigation of the Ca^{2+}–N_2 and Ca^{2+}–N_2 complexes. Chem Phys Lett 295:204–210
40. Baruah B, Swafford LA, Crans DC, Levinger NE (2008) Do probe molecules influence water in confinement? J Phys Chem B 112:10158–10164
41. Rode BM, Schwenk CF, Hofer TS, Randolf BR (2005) Coordination and ligand exchange dynamics of solvated metal ions. Coord Chem Rev 249:2993–3006
42. Adeagbo WA, Doltsinis NL, Burchard M, Maresch WV, Fockenberg T (2012) Ca^{2+} solvation as a function of p, T, and pH from ab initio simulation. J Chem Phys 37:124502
43. Carlotti B, Cesaretti A, Elisei F (2012) Complexes of tetracyclines with divalent metal cations investigated by stationary and femtosecond-pulsed techniques. Phys Chem Chem Phys 14:823–834